Hybrid-bubble-chamber study of nucleon diffractive dissociation in 14-GeV/c $\pi^{\pm}p$ collisions

G. B. Chadwick, J. T. Carroll, V. Chaloupka, J. Ballam, J. Bouchez,* P. Herquet,† D. Linglin,‡ K. C. Moffeit, and R. Stevens

Stanford Linear Accelerator Center, Stanford University, Stanford, California 94305

V. Davidson, A. Firestone,§ F. Nagy, C. Peck, and L. Rosenfeld

California Institute of Technology, Pasadena, California 91125

R. Ely, D. Grether, and P. Oddone

Lawrence Berkeley Laboratory, Berkeley, California 94720

(Received 6 October 1977)

Two experiments to study the low-mass diffractive enhancement recoiling against a fast forward pion from π^+p and π^-p collisions at 14 GeV/c are described. Photographs of the SLAC 40-in. hydrogen bubble chamber were triggered by a downstream spectrometer when the missing mass, calculated on-line, was above 1.1 GeV. Evidence for a nonresonant mass peak at 1.35 GeV is presented, as well as for production of resonances at about 1.5 and 1.68 GeV. The data are presented as distributions in mass and momentum transfer, as well as moments and isocline plots of the decay angular distributions. Model-independent features are emphasized.

I. INTRODUCTION

We have performed two experiments in which about 227 000 πp inelastic scattering events were measured in order to study the detailed nature of the low-mass enhancement recoiling against the fast forward pion in these events. This enhancement appears to be produced by all hadron beams over a very wide energy range with comparable cross sections and is generally supposed to be the result of diffractive scattering or Pomeron exchange. For three-body final states the simplest processes are illustrated in Fig. 1. These are: (a) direct-nucleon-pole contribution, (b) pion exchange with $\pi\pi$ scattering, (c) baryon exchange with πN scattering, and (d) nucleon-resonance excitation.

Although from the earliest studies of the process it was recognized that resonancelike structures appear in the enhancement, no clear identification of the mass peaks has been made.[1] Attention turned to the Drell-Hiida[2] or Deck[3] (DHD) effect of diagram (b), which can be made to describe the gross features of the data, especially if form factors and absorption corrections are introduced.[4] Recently, the possible importance of nucleon exchange has been stressed.[1,5,6] It has been shown[5,6] that contributions from (a) and (c) tend to cancel, which may explain the relative success found using (b) alone, but which also suggests that much more detailed data will be needed than heretofore to identify the individual contributions from the processes of Fig. 1.

In our experiments, the SLAC 40-in. hydrogen bubble chamber was run at a high repetition rate while exposed to 14-GeV/c π^+ and π^- beams. Photo-

graphs were taken only when a fast forward scattered particle, corresponding to that expected from the inelastic diffraction process, was detected in a large acceptance magnetic spectrometer downstream. In the 2–3 msec between beam passage and full bubble growth, it was possible to calculate the apparent missing mass recoiling against the detected pion and, thus, exclude most of the prolific elastic scattering events. Furthermore, this hybrid system allowed the fast particle to be measured with much higher precision than could be obtained with the bubble chamber alone, which resulted in our obtaining a data sample with very small contamination from multineutral events.
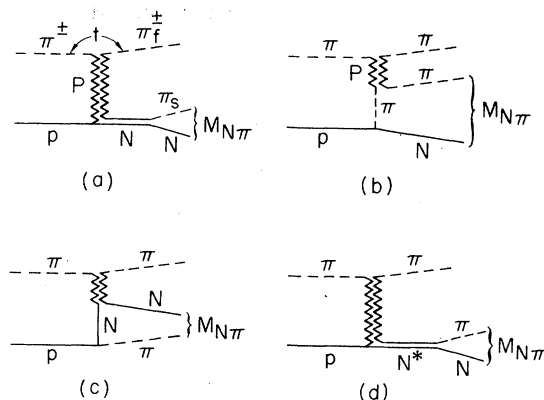

FIG. 1. Diagrams of the exchange processes expected to contribute to the diffractive low-mass enhancement in proton dissociation: (a) baryon-exchange direct nucleon pole, (b) pion-exchange DHD effect, (c) baryon-exchange DHD effect, (d) nucleon-resonance production.

In this paper we present our observations of the following reactions (the diffractively produced system is shown here in parentheses):

$$\pi^+ p \to \pi^+ (p\pi^\circ) , \tag{1}$$

$$\pi^- p \to \pi^- (p\pi^\circ) , \tag{2}$$

$$\pi^+ p \to \pi^+ (n\pi^+) , \tag{3}$$

$$\pi^- p \to \pi^- (n\pi^+) , \tag{4}$$

$$\pi^+ p \to \pi^+ (\Delta^{++}\pi^-) , \tag{5}$$

$$\pi^- p \to \pi^- (\Delta^{++}\pi^-) . \tag{6}$$

For convenience we shall use the notation $\pm (p\pi^\circ)$, $\pm (n\pi^+)$, and $\pm (\Delta\pi)$ to refer to these pairs of reactions.

At our energy we can attempt to interpret the interference between the already important diffractive, and not yet negligible nondiffractive processes, using their dependence on the charge of the beam. At this time we will present mainly the data itself. A more detailed analysis is in progress.

II. EXPERIMENTAL DETAILS

The layout of the hybrid system used in this experiment is shown in Fig. 2. A pion beam of 14-GeV/c nominal momentum (14.2 GeV/c for π^-, 13.7 GeV/c for π^+) traversed the SLAC 40-in. hydrogen bubble chamber which was equipped with thin windows for particle entry and exit and which could run at up to 12 expansions per second. The scattering of a beam pion in the horizontal plane was detected by a coincidence between scintillation counters S_B, S_1, and S_2. The latter two scintillators were divided into left and right sections, separated so that the undeflected beam would pass between them undetected. A coincidence produced a spark-chamber trigger for four "stations" of magnetostrictive wire spark chambers (WSC), which were read into a SIGMA 2 computer. A dipole magnet of approximately 2.8-T m bending power was used. Each station contained a pair of horizontal (x) and vertical (y) wire planes and, in addition, stations 1 and 3 each had a pair of planes with wires at $\pm 45°$ to the vertical to resolve multispark ambiguities. In the π^+ experiment, the wire
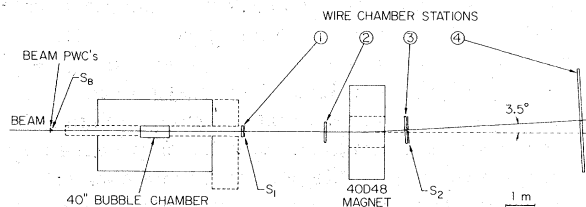

FIG. 2. Layout of the hybrid-bubble-chamber system.

hits in two proportional wire chambers (PWC) caused by the beam particle were also read in; these chambers were not available for the π^- exposure. Some further details of the apparatus may be found in Ref. 7.

After the wire-chamber hits were read into the computer, there remained approximately 2 msec, while bubbles were growing in the bubble chamber, before a decision to flash the camera lamps had to be made. The following algorithm was used on the spark-chamber data to define a computer trigger:

(i) Search the horizontal wands of the wire spark chambers 1 and 2 for segments which pass through the center of the bubble chamber within a broad tolerance. Extrapolate each such segment to the center of the dipole. Next, search stations 3 and 4 for segments which have the same intercept at the dipole.

(ii) Use the dipole bend angle and the scattering angle projected on the horizontal plane (containing the bubble-chamber field), θ_x, to estimate the missing mass (MM):

$$\text{MM}^2 = M_p^2 + 2M_p(E_{\text{beam}} - E_{\text{fast}})$$

$$- P_{\text{beam}}P_{\text{fast}}\theta_x^2 , \tag{7}$$

where the beam is assigned fixed values determined periodically.

(iii) Apply the first trigger condition: $1100 < \text{MM} < 3500$ MeV. Since the elastic cross section is about 5 mb and the diffractive cross section is about 1 mb, the experiment would be swamped with elastics if the accuracy of MM is not sufficient to reject them. The spread in beam momentum was less than 0.5% and the error in P_{fast} was about the same. Hence, the on-line error in MM is about 100 MeV including the error due to neglecting the scattering angle normal to the bubble-chamber field. The minimum of 1100 MeV was set to reject about 75% of the elastics at the sacrifice of a reduced efficiency for masses near 1100 MeV.

(iv) For the final trigger condition, require the track to intercept the center of the bubble chamber to ± 1.5 cm in the horizontal plane. The horizontal width of the beam of 0.5 cm, the length of the fiducial area of 75 cm, and the maximum horizontal acceptance of ± 60 mr guarantee that legitimate interactions satisfy this criteria. This is not sufficiently tight to reject many interactions in the windows, but it was necessary to reduce triggers by the muon halo from decays upstream.

Because the wire spark chambers were sensitive to particles over most of the 1.5-μsec beam spill, those wires in the region of the unscattered beam (i.e., between the halves of the trigger counters S1 and S2) were desensitized. For this reason the useful limit of $|t|$ was 0.01 GeV^2. The upper limit,

set by apertures, was 0.6 GeV^2.

The system could accommodate up to 10 particles per expansion. At this rate there was an average of 2 sparks in the last plane, and the computer finished scanning in an average of 0.8 msec. In early runs, 10% of the spark-chamber triggers required more than 2 msec to analyze, and these were rejected outright. Later improvements reduced this loss to only a few percent.

Approximately 0.8% of beam particles triggered the flashes, and of the resulting film, 30% of frames contained good events within the fiducial volume. For the first π^- exposure, the bubble-chamber expansion rate was 2/sec. Through the efforts of the SLAC Bubble Chamber Operations Group, this rate was increased to 12/sec later.

III. DATA ANALYSIS

To obtain the data sample to be discussed, the film was scanned for two- and four-prong events in the fiducial volume. Both normal and "directed scan" techniques were used. In the directed mode, the spark-chamber data were used to predict the position on the projected views of the triggering track near the bubble-chamber exit window. With this information, the scanners could reject events occurring accidentally along with a triggering event (real or spurious) and find real events with improved efficiency.

Events were measured on the LBL flying-spot digitizer and COBWEB system, the SLAC spiral reader and conventional systems, and on the Caltech POLLY. Measurements were accepted for events with a track matching one found in the downstream spectrometer. The matching procedure consisted of the following steps: (i) Locate all possible track projections in both horizontal and vertical planes, and associate these using the 45°-wire-plane sparks at stations 1 and 3. (ii) Project all candidate trajectories and their errors to the position of the event vertex as measured on the film, through the known bubble-chamber fringe field. (iii) Reject "spark-chamber tracks" which fail to match the coordinates of the vertex, and test the remainder for compatibility of angles and momentum, selecting the best match χ^2. (iv) Form a "hybrid track" with production angles, momentum, and error matrix taken as the weighted average between bubble-chamber and projected spark-chamber measurements.

The "hybrid" track resulting from this procedure generally had a momentum error of ±80 MeV/c and angle errors of the order ±0.5 mr. In the π^+ experiment the beam track was also matched to the upstream proportional chamber hits, using a procedure similar to the downstream matching. If the beam track was compatible with the mean beam parameters, the measurement was averaged with those mean values. This resulted in comparable errors on beam and outgoing fast particle.

Each event was processed through SQUAW where 4C, 1C, and 0C fits were made. For those events giving an acceptable 4-constraint (4C) fit, the 1C and 0C fits were ignored. Reactions 1–4 studied here are 1C fits. Only 1C fits with probability greater than 5% were accepted; cross sections were corrected to account for this rejection. For ambiguous events between a proton and pion hypothesis we selected the "correct" fit by the following criteria:

(i) Backward tracks in the laboratory and tracks identified by δ rays were called pions. Stopping tracks were called protons.

(ii) If the questionable track was greater than 15 cm, the film root-mean-squared deviation (FRMS) was used to select the appropriate hypothesis when the Δ(FRMS) > 4 microns and Δ(FRMS)/Σ(FRMS) > 0.25.

(iii) Fits with tracks having $p > 1.2$ GeV/c or dip > 40° were selected by using the fit with the highest confidence level probability. After these selections, events remaining with ambiguous interpretations were checked for compatibility with the predicted ionization, as obtained automatically in the measuring process or as estimated visually.

IV. CROSS-SECTION DETERMINATION

Each event was assigned a weight proportional to the inverse of its geometrical acceptance, calculated as the fraction of trigger-particle orbits traversing active areas of the WSC's when the azimuth for that particular track was rotated about the beam direction. The average behavior of the acceptance is shown in Fig. 3 as a function of missing mass and t. In addition, a correction for the on-line rejection of low-missing-mass events as elastics was applied. The weight was finally divided by the total exposure sensitivity, in events/μb.

In order to determine the effective beam flux in both experiments in a consistent way, we made use of published elastic scattering cross sections, which are well determined at our energies.[7,8] Periodically, throughout the runs, the missing-mass requirement was changed to allow all elastic events to trigger. The resulting "elastic rolls" of film were scanned and measured using the same criteria as for production film. The elastic events found were used to check that the event weights obtained from the acceptance calculation produced a t distribution compatible with that from counter measurements, and the beam flux for elastic rolls was determined by normalizing the cross section
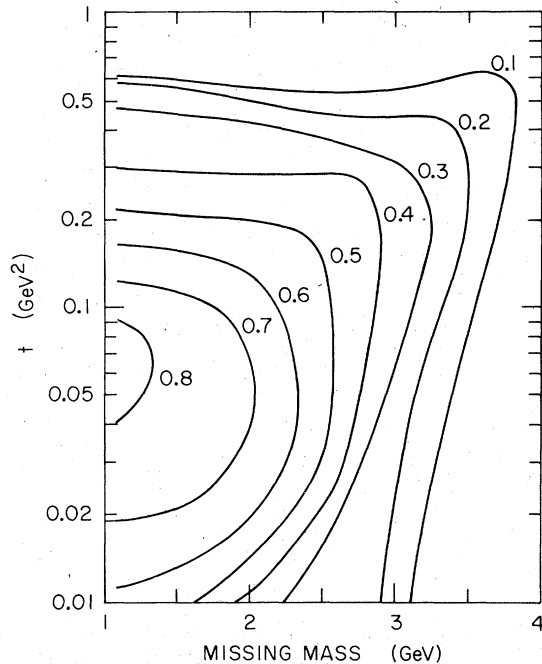
FIG. 3. Average geometrical acceptance of the system as a function of missing mass and t.

V. EVENT SELECTION

The selection of $\pi^{\pm}p \to \pi^{\pm}p\pi^{+}\pi^{-}$ events by 4-constraint (4C) kinematic fits presented no problems. In contrast, the 1C-fit channels could be contaminated by elastic events failing the 4C fit because elastic scatters produced 15 times more spark-chamber triggers than the $\pm(p\pi^{\circ})$ reaction. 75% of these were rejected by the computer trigger: The remainder had to be excluded using the measurements on film. Four-constraint fits were tried on all two-prong events, first using the hybrid measurements, and then using only the bubble-chamber values. About 5% of elastics producing spark-chamber triggers failed the hybrid fit. This fraction can be explained by the trigger track interacting in the bubble-chamber windows or spectrometer. Therefore, "bubble-chamber-only" fits were used to exclude elastics. Finally, 0.4% of all elastics failed all 4C fits. These were excluded by a coplanarity test.

1C-fit events were selected on the basis of the best χ^{2}, after elastic events were excluded and ionization selection applied. The quality of the resulting samples can best be illustrated by the missing neutral mass (squared) found for all candidates for
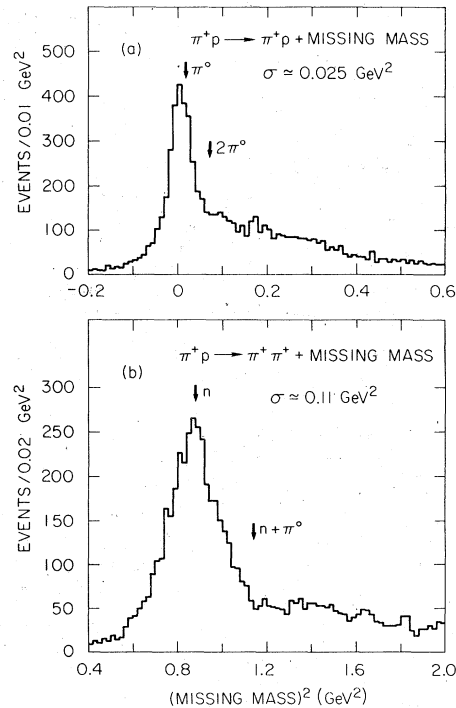
for $0.05 < |t| < 0.3$ GeV to the published values.[8] The flux for the entire experiment was determined by multiplying the "elastic-rolls" flux by the ratio of the number of all 2- and 4-prong events with missing mass above 1.4 GeV, to that for elastic rolls only. By using this procedure we estimate that the relative normalization between π^{+} and π^{-} exposures is uncertain to about ±8% (3% statistical error). In principle, all inefficiencies in the electronic detectors and on-line event selection, as well as in the scanning and measuring procedures, should be the same in both experiments.

The fit-selection process can also contribute to the uncertainty in the cross sections. The contamination from other reactions is larger at higher nucleon-pion masses and for decays with the charged particle forward. In addition, the π^{-} and the π^{+} experiments were processed by different groups. We estimate the uncertainty in cross sections between the π^{+} and π^{-} data at ±5% due to the fit-selection procedures. In addition, within each experiment the contamination and loss of fits is estimated to be less than 20% in any different mass or angular region.

The resulting sensitivities for the π^{+} and π^{-} exposures respectively were 95 and 79 weighted events/μb. (In both experiments the weight averaged over all events was about 1.8.) As discussed below, we estimate that an uncertainty of ±15% should be assigned to the absolute cross sections.

FIG. 4. Missing mass squared calculated for inelastic two-prong events compatible with the reactions (a) $\pi^{+}p \to \pi^{+}p + MM$ and (b) $\pi^{+}p \to \pi^{+}\pi^{+} + MM$, after ionization selection. Single-neutral mass and multi-neutral thresholds are shown by arrows.

reactions $\pi^+ p \rightarrow \pi^+ p + $ MM and $\pi^+ p \rightarrow \pi^+ \pi^+ + $ MM, as shown in Fig. 4. Similar results were obtained for the π^--induced samples. We estimate that about 10% of events selected as good 1C fits will in fact have more than one neutral, while a similar number of single neutrals will fail the fit. From the study of elastic fits discussed above, we expect 5% of inelastic events also to have a bad measurement on either the beam or outgoing track. Most of these will still fit the 1C hypothesis. All these considerations lead us to assign a ±15% error to the absolute cross sections, while the parallel treatment of π^+ and π^- data allows a smaller error to be placed on the relative normalization.

VI. DETAILED PROPERTIES OF THE $\pm(p\pi^\circ)$ AND $\pm(n\pi^+)$ CHANNELS

A. Mass spectra

In Fig. 5(a) we show the nucleon-π mass spectra for the $\pm(p\pi^\circ)$ channels for $0.01 < |t| < 0.5$ GeV^2. Events in this and subsequent plots are weighted as described in Sec. IV. Error bars are statistical only. There is close agreement in both cross section and mass structure in these reactions when integrated over all the angles. In Fig. 5(b) we show similar plots for the $\pm(n\pi^+)$ channels. Here
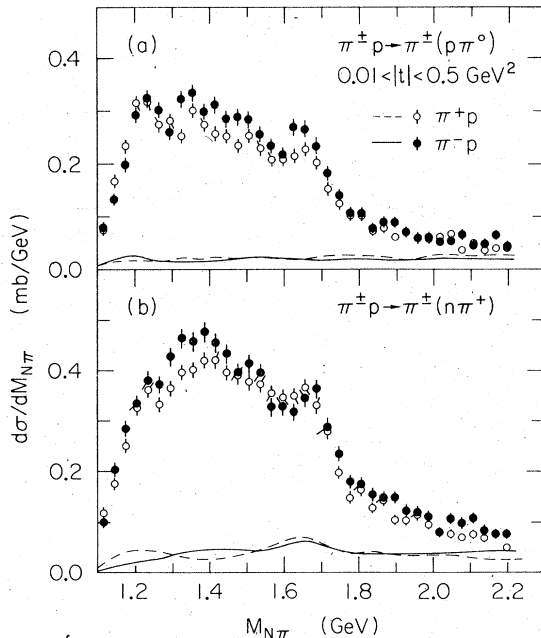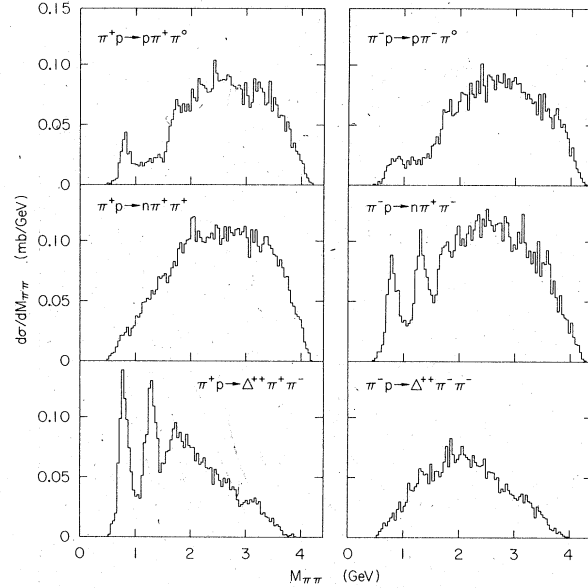

FIG. 6. Dipion mass spectra for the six reactions considered. The t cut is the same as for Fig. 5, and $M_{N\pi} < 2$ GeV.

FIG. 5. Nucleon-pion invariant-mass spectra, weighted for acceptance, found in the π^+ (open circles) and π^- (closed circles) experiments for the reactions (a) $\pi^\pm p \rightarrow \pi^\pm (p\pi^\circ)$ and (b) $\pi^\pm p \rightarrow \pi^\pm (n\pi^+)$. Solid and broken lines show the π^- and π^+ data, respectively, for $M_{\pi\pi} < 1.5$ GeV.

we observe an excess of π^- over π^+ induced reaction cross sections.

In Fig. 6 we show the dipion mass spectra for the same data for $M_{N\pi} < 2$ GeV. The $M_{\pi\pi}$ spectra for $\pm(\Delta\pi)$ channels are also plotted for later reference. Here we see that production of ρ, f, and g resonances are important contributions to those channels allowed by isospin. However, there is only minor overlap of dipion resonances with the $N\pi$ diffractive enhancement. This is shown in Fig. 5, where the general level of ($N\pi$) cross sections with $M_{\pi\pi} < 1.5$ GeV are shown by broken and solid lines for the $+(N\pi)$ and $-(N\pi)$ channels, respectively.

The ρ signal in the $+(p\pi^\circ)$ channel is more clearly defined than in the $-(p\pi^\circ)$ channel. This is because the ρ in these channels is produced opposite a slow, wide angle proton which makes the mass resolution particularly sensitive to the angular measurements of the fast tracks. In the π^+ experiment the use of wire chambers to define the incident beam made a substantial improvement in resolution at low $\pi\pi$ mass. For higher dipion mass, the error falls like $M_{\pi\pi}^{-1}$ and soon becomes less than the resonance widths. In addition, the kinematic overlap of ρ production with the ($N\pi$) low-mass region is small, and so the poorer resolution in the π^- data should not affect that analysis.

The agreement between $\pm(p\pi^\circ)$ mass spectra [Fig. 5(a)] in magnitude and shape is not surprising. Referring to Figs. 1(a) and 1(d), with the Pomeron replaced by all possible exchanges, difference
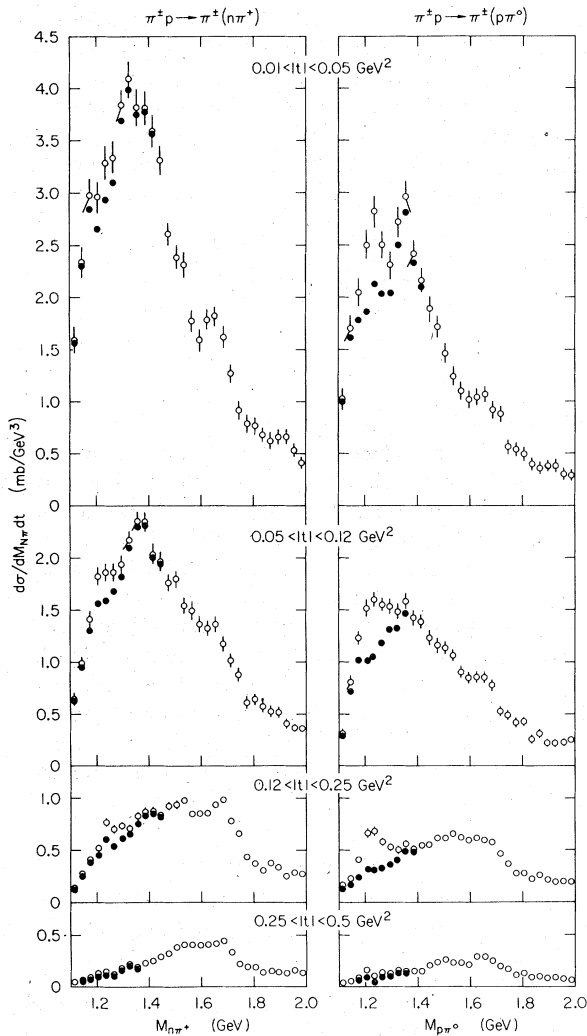
FIG. 7. Average $d\sigma/dM_{N\pi}dt$ for $\pi^{\pm}p \to \pi^{\pm}(p\pi^{\circ})$ and $\pi^{\pm}p \to \pi^{\pm}(n\pi^{+})$ in four t intervals (open circles). Closed circles show the result of subtracting the known Δ^{+} contribution in each case.

should arise from the interference between $I = 0$ and 1 exchange, and previous experiments have shown these terms (averaged over decay angles) to be small.[9] For the processes of Figs. 1(b) and 1(c), $\pi^{\pm}\pi^{\circ}$ scattering cross sections are identical, and $\pi^{\pm}N$ cross sections are similar in the mass region imposed by our cuts. In the $(n\pi^{+})$ channels, by the same token, differences can be most reasonably attributed to the inequality of $\pi^{+}\pi^{+}$ and $\pi^{+}\pi^{-}$ scattering.

We now form the average $d^2\sigma/dM_{N\pi}dt$ for positive and negative beams. This procedure has two virtues: (1) interference between $I = 0$ and $I = 1$ exchange processes will cancel before averaging over decay angles, and (2) statistical fluctuations decrease. In Fig. 7 we plot the averaged cross sec-

tions (open circles) for $(n\pi^{+})$ and $(p\pi^{\circ})$ reactions against $M_{N\pi}$ in four intervals of t. The data show a very strong t dependence, especially at very low nucleon-pion masses.

In all these spectra we see clear evidence of Δ^{+} (1232) production, which cannot be diffractive. We, therefore, subtract it out, using data from a high-statistics experiment which studied the reaction

$$\pi^{+}p \to \pi^{\circ}\Delta^{++} \to \pi^{\circ}(p\pi^{+}) \tag{8}$$

at 13.1 GeV/c,[10] and found $\sigma_{\Delta^{++}} = 45 \pm 7$ μb. Isospin invariance indicates that in reactions (1) and (2) the cross section for

$$\pi^{\pm}p \to \pi^{\pm}\Delta^{+} \to \pi^{\pm}(p\pi^{\circ}) \tag{9}$$

should be $\frac{4}{9}$ that of reaction (8), while for $\Delta^{+} \to n\pi^{+}$ we should find a factor of $\frac{2}{9}$ applies. Using the data of Ref. 10 and a Breit-Wigner shape for the Δ^{+}, we show the result of the subtraction by closed circles on each section of Fig. 7.

This procedure results in the appearance of a "shoulder" under the position of the Δ^{+}, followed by a clear peaking at mass 1.35 GeV.[11] This peak rapidly diminishes as $|t|$ is increased, and vanishes for $|t| > 0.12$ GeV^2.

The next most salient feature of the data shown in Fig. 7 is the presence of a peak at 1.65-GeV mass, followed by a sharp drop at about 1.7 GeV. In this case, the effect shows a comparatively weak t dependence.

Finally, we note that no clear mass structure between the 1.35- and 1.65-GeV peaks is visible in any of the kinematic regions shown.

B. Comparison with CERN ISR results

A comparison of our mass spectra at $\sqrt{s} = 5.2$ GeV with a closely related reaction at very high energy proves to be very interesting. The process

$$pp \to p(n\pi^{+}) \tag{10}$$

has been studied[12,13] using the CERN split-field-magnet facility of the ISR. We have already reported on the striking similarity of the low-mass $(n\pi^{+})$ enhancement in reaction (10) at $\sqrt{s} = 53$ GeV and in our data.[14] Here we wish to repeat the comparison using the newer ISR data at $\sqrt{s} = 45$ GeV.[13] In Fig. 8 we show our mass spectra, $d\sigma/dM$, averaged between + $(n\pi^{+})$ and – $(n\pi^{+})$ channels, for 0.05 $< |t| < 0.5$ GeV^2, superimposed upon the spectra of reaction (10) (upper histograms) 0.05 $< |t| < 0.8$ GeV^2. In both cases the data are divided into forward [$\cos\theta > 0$, Fig. 8(b)] and backward [$\cos\theta < 0$, Fig. 8(a)] decay angles in the Gottfried-Jackson system defined in the next section.

It is remarkable that these mass spectra are so similar, despite the factor of 10 difference in
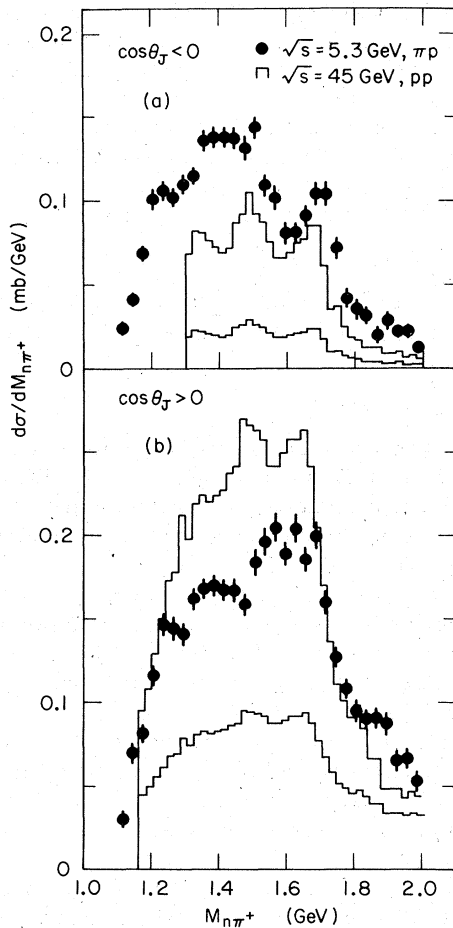
FIG. 8. (a) Average $d\sigma/dM_{n\pi^+}$ for $\pi^\pm p \to \pi^\pm (n\pi^+)$ (closed circles), with $0.05 < |t| < 0.6$ GeV^2, obtained in this experiment, compared to that for $pp \to p (n\pi^+)$ at $\sqrt{s} = 45$ GeV, $0.05 < |t| < 0.8$ GeV, $\cos\theta_J > -0.9$, obtained at the ISR (Ref. 13, higher histogram), for backward neutron decay angle in the t-channel frame. Nonoverlap indicates a mass cutoff imposed on the ISR data by acceptance. The lower histogram shows the "factorization normalized" cross section defined by Eq. (11). (b) Same comparison for forward decay neutrons.

c.m.s. energy and the different projectiles involved. For $\cos\theta > 0$ the smooth rise of $d\sigma/dM$ with M, followed by a sharp drop at 1.7 GeV, is almost identical. For $\cos\theta < 0$ both data show enhanced mass structure: The effect at 1.65 GeV is particularly striking in similarity. In the ISR data a peak at 1.5 GeV is evident: In our data it is much less compelling. However, we will see in a later section that our data also indicate the presence of a resonance at this mass.

Continuing the comparison, we note from Fig. 8 that the high-energy data show a strong forward asymmetry in the decay angular distribution at all masses. The πp data show a similar but less

strong forward asymmetry. Since in both data sets the mass peak structure is so similar, this suggests that it is the background under the peaks which produces the increased angular asymmetry at high energy.

Finally, we calculate the "factorization normalized" cross section for the pp data, as defined in Ref 14:

$$\frac{d\sigma_N(s)}{d_M} = \frac{\sigma(\pi p \text{ elastic}, \sqrt{s} = 5.2 \text{ GeV})}{2\sigma(pp \text{ elastic}, \sqrt{s})}$$

$$\times \frac{d\sigma}{dM} (pp \text{ inelastic}, \sqrt{s}). \tag{11}$$

This formula uses the elastic cross sections to account for the difference between pion-Pomeron and proton-Pomeron coupling, as well as the s dependence of the Pomeron propagator, in the spirit of factorization of Regge amplitudes. The factor of 2 in the denominator accounts for the fact that there are two vertices from which a low-mass $n\pi^+$ may be produced in pp collisions and only one in πp collisions. The normalized pp cross section is shown in Fig. 8 (lower histogram). The comparison shows that the overall cross section of the diffraction enhancement does not follow the elastic cross section so that this form of factorization is not exact.

C. Angular distributions

To describe the angular distribution of the $(N\pi)$ system, we define unnormalized moments as follows:

$$Y_l^m = \frac{1}{f\Delta M_{N\pi}} \sum_{N\pi \text{ events}} w_i \text{Re} Y_l^m(\theta_i, \phi_i), \tag{12}$$

where f is the exposure sensitivity given previously, $\Delta M_{N\pi}$ is the mass bin width, w_i is the weight of the ith event, and θ_i, ϕ_i are the polar and azimuthal angles of the nucleon in the center of mass of the nucleon-slow π system. The angles are defined in the Gottfried-Jackson system,[15] where the z axis is taken along the direction of the incident nucleon, y is along the normal to the production plane,

$$\hat{y} \sim \vec{\pi}_{\text{inc}} \times \vec{\pi}_{\text{fast}},$$

and $\tag{13}$

$$\hat{x} \sim \hat{y} \times \hat{z}.$$

The most significant moments obtained using Eq. (12) are shown in Fig. 9. Here we have divided the data into two t bins, i.e., $0.01 < |t| < 0.12$ GeV^2 and $0.12 < |t| < 0.5$ GeV^2, so that the 1.35-GeV peak will be dominant in the first bin and relatively insignificant in the second. Δ production divides equally between the two bins. Finally, we have superimposed the π^+- and π^--induced results to accentu-

$\pi^{\pm}p \rightarrow \pi^{\pm}(p\pi^{\circ})$ $\pi^{\pm}p \rightarrow \pi^{\pm}(n\pi^{+})$ $\pi^{\pm}p \rightarrow \pi^{\pm}(p\pi^{\circ})$ $\pi^{\pm}p \rightarrow \pi^{\pm}(n\pi^{+})$

0.01 < |t| < 0.12 GeV^2 0.12 < |t| < 0.5 GeV^2

$\langle Y_{\ell}^m \rangle \, d\sigma/dM_{N\pi}$ (μb/GeV)

Y_1^0 Y_1^1 Y_2^0 Y_2^1 Y_2^2 Y_3^0 Y_4^0 Y_5^0 Y_6^0
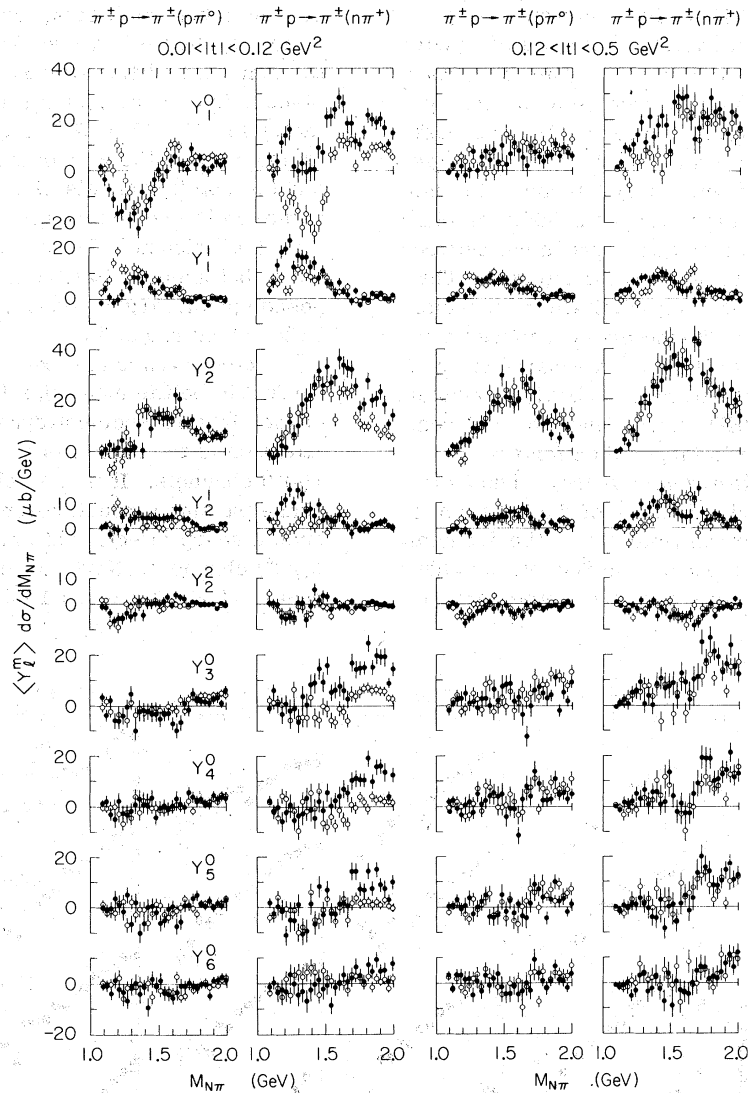
$M_{N\pi}$ (GeV) $M_{N\pi}$ (GeV)

FIG. 9. Unnormalized moments of the nucleon decay angle, °in the t-channel frame, for the reactions and t intervals shown. π^+-beam results are shown by open circles, π^- by closed circles.

ate isospin interference effects.

These data show a very complex behavior. In order to simplify the discussion we now give a qualitative description of those features which appear consistently through all the channels.

(a) Δ *interference effect.* In the region of the $\Delta(1232)$ we observe that the Y_1^0, Y_1^1, and Y_2^1 moments change with the charge of the beam. In the + $(p\pi^{\circ})$ channel they peak to positive values roughly at the Δ mass, and to negative values in the $-(p\pi^{\circ})$ channel. The effect also changes sign in going from proton to neutron channel, while the magnitude is roughly constant. Finally, Y_2^0 also indicates that interference is present, while the Y_2^2 difference is consistent with zero.

An analysis of these Δ interference effects has already been published[16] based on preliminary data from this experiment. There it was shown that the data are best explained by a model in which the Δ amplitude ($I = 1$ exchange) interferes with an $I = 0$ exchange s- and p-wave background.

(b) *High-mass region.* For $M_{N\pi} > 2$ GeV (off scale in Fig. 9), the moments tend to show a smooth behavior. For lower l, this plateau is reached earlier. For $m \neq 0$ the values here are compatible with zero, while for $m = 0$ they tend to be positive. This behavior results from the strong peaking of the angular distribution at $\theta = 0$ in the t-channel helicity system, which contributes to all $m = 0$ moments. The most likely explanation of

such peaking is the DHD-effect diagram of Fig. 1(b), which implies a small 4-momentum transfer between target and recoil proton. This reflects into the $N\pi$ center-of-mass system as a peaking near $\cos\theta = 1$, becoming sharper as $M_{N\pi}$ increases.

(c) *The* $-(n\pi^+)$ *channel at low t.* There is a general agreement in magnitude and shape of the moment distributions in the $\pm(p\pi^\circ)$ channels for $M_{p\pi^\circ}$ > 1.4 GeV. There is also good agreement between the $\pm(n\pi^+)$ channels in the higher-t interval. The $-(n\pi^+)$ channel for $0.01 < |t| < 0.12$ GeV^2, therefore, appears anomalous in having moment values considerably in excess of their counterparts in the $+(n\pi^+)$ channel. This effect is probably attributable to the π-exchange DHD effect, since the $\pi^+\pi^-$ scattering cross section is larger than for $\pi^+\pi^+$.

(d) *Forward-backward asymmetry.* The $l = 1$ moments give a good indication of the behavior of the forward-backward asymmetry in the decay angular distribution referred to in Sec. VI B. There we noted that the general forward asymmetry, ob-

served in both data sets, was considerably stronger in the ISR pp data (see Fig. 8). Here we wish to point out that the forward asymmetry is replaced, in our data, by a strong backward asymmetry for $M_{N\pi} < 1.5$ GeV and $|t| < 0.12$ GeV^2. This is observed in the Y_1^0 moment of Fig. 9 in the $\pm(p\pi^\circ)$ and the $+(n\pi^+)$ channels as a smooth dip to negative values in the region of the 1.35-GeV mass peak. In the $-(n\pi^+)$ channel, Y_1^0 does not actually go negative here, but appears to have a negative dip superimposed upon a larger positive background than found in the other channels.

(e) *Interference patterns.* We now point out what we feel to be the most significant evidence for resonance interference patterns in Fig. 9. We direct attention to the rapid rise in Y_1^0 at $M = 1.5$ GeV in the $\pm(n\pi^+)$ channels. It is unlikely that anything but a phase passing through resonance could produce such a sharp effect. This rise is less sharp in the $\pm(p\pi^\circ)$ channels. Next, we note that Y_2^0 shows two peaks, at about 1.5 and 1.65 GeV, but shows no
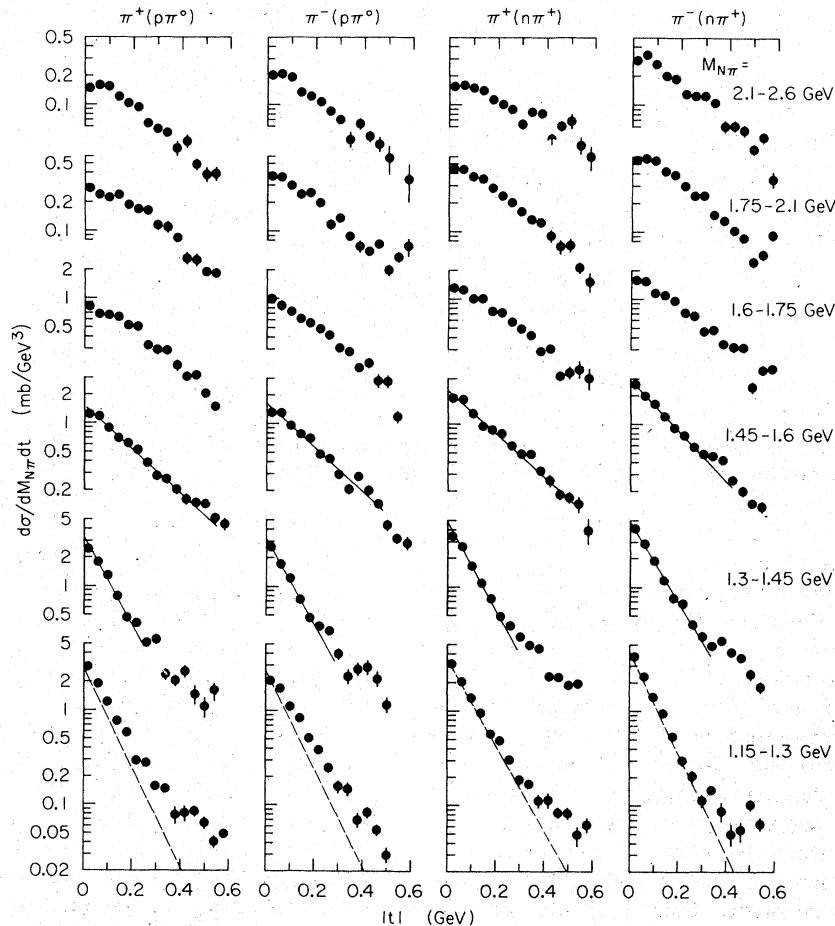

FIG. 10. t distributions for various $M_{N\pi}$ regions indicated at right, for the reaction channels shown above. Solid lines indicate the e^{Bt} dependence, broken lines show the same after Δ^+ has been subtracted.

structure at 1.35 GeV. Finally, what appears to be a resonance interference pattern in Y_4^0 and Y_5^0 appears at about 1.7 GeV, while another occurs in Y_4^0 at 1.5 GeV. Y_4^0 shows an indistinct rise at 1.65 GeV, but it is not clear whether this should be associated with the peak at that mass, or considered part of the pattern centered at 1.5 GeV.

In the moments with $m \neq 0$ we find some evidence for interference patterns, which suggests that at least some components of the production amplitudes do not conserve t-channel helicity. These terms appear to be rather small compared to the $m = 0$ signals. When the moments were plotted in the s-channel helicity frame, the $m \neq 0$ moments generally became very large. Since the helicity structure is relatively more simple in the t-channel frame, we shall continue to use it for analysis.

D. *t* dependences

Figure 10 shows the t dependence of the cross section for all four channels and for six mass bins. The mass bins were chosen so that each contains
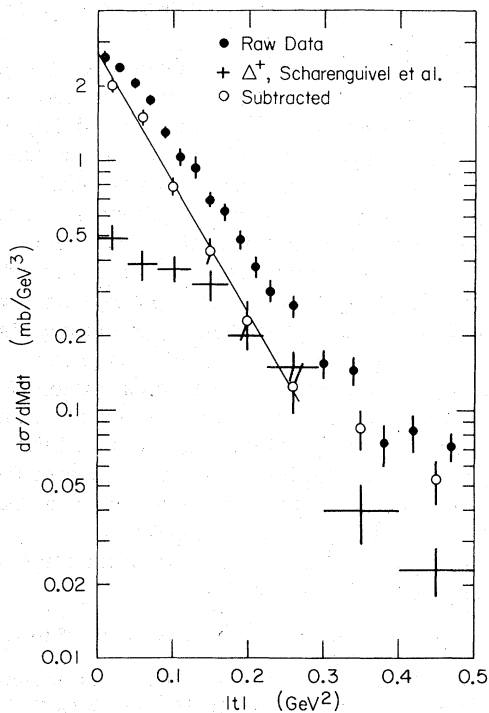

FIG. 11. Illustration of the composition of the lowest mass bin, $1.15 < M_{p\pi^0} < 1.3$ GeV, for the average $d\sigma/dMdt$ for $\pi^\pm p \to \pi^\pm (p\pi^0)$. Crosses show the data of Ref. 10 multiplied by the isospin factor $\frac{4}{9}$, and the open circles show the result of subtracting this from our average data (closed circles). Note that the slope of the solid line fitted to the open circles will be strongly dependent on the relative normalization of the two experiments.
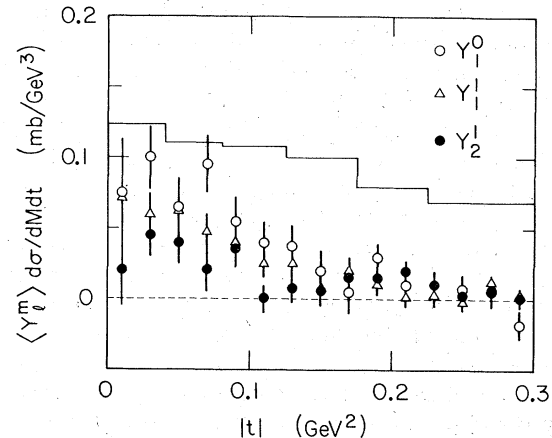

FIG. 12. Interference moments of the Δ with its "background" as function of t, obtained by subtracting moments for $\pi^- p \to \pi^- (p\pi^0)$ from $\pi^+ p \to \pi^+ (p\pi^0)$ moments in the interval $1.15 < M_{p\pi^0} < 1.3$ GeV. Histogram shows $(d\sigma_\Delta/dt)^{1/2}$ from Ref. 10.

one of the features of the moment distribution mentioned in Sec. VI C. The well-known mass-slope correlation is evident here. The solid lines are the result of fits assuming a pure exponential dependence e^{Bt}. In the lowest mass bin the Δ^+ was subtracted before fitting, as explained below.

At low $N\pi$ mass, the $d^2\sigma/dMdt$ is well described by the exponential in t; for higher masses a flattening of the distribution at low t is observed. We also note that the dip at $|t| \sim 0.2$ GeV², reported at higher energies,[13,17] is weaker here, or absent. More quantitative results will be given in Sec. VIII C.

In the interval $1.15 < M_{p\pi^0} < 1.3$ GeV we have subtracted the Δ^+ contribution. This is illustrated by Fig. 11, where the average $d\sigma/dMdt$ for reactions (1) and (2) is shown together with the Δ distribution expected in the interval, based on the data of Scharenguivel *et al.*[10] The subtracted distribution shows a exponential shape with slope parameter[11] $B = 12 \pm 0.5$ GeV⁻². The fitted non-Δ exponential distribution for this mass bin is also shown in Fig. 10 by a broken line.

We now consider the t dependence of the interference moments Y_1^0, Y_1^1, and Y_2^1 of the Δ with the background. These are obtained by plotting one-half the difference between $+(p\pi^0)$ and $-(p\pi^0)$ moments in the Δ interval $1.15 < M_{p\pi^0} < 1.3$ GeV. Figure 12 shows $\langle Y_l^m \rangle d\sigma/dMdt$ for these moments plotted against t. The histogram shows the expected Δ amplitude (square root of $d\sigma_\Delta/dt$ obtained from Ref. 10) with arbitrary normalization. If we assumed that the Δ^+ is produced via the Stodolsky-Sakurai (SS) mechanism,[18] we would conclude that the strong t dependence in the $l = 1$ moment re-

flected that of the background amplitude. However, an alternative interpretation is that the Δ^+ develops a strong helicity nonflip component at small t, as has been suggested by Krammer and Maor.[19] We will term this the KM mechanism.

The Y_1^0 and Y_1^1 moments show very similar behavior and do not turn over at small t. This confirms the observation of Scharenguivel et al.[10] that the Δ amplitude has no forward dip. It also suggests that the s-wave background is finite at small t. The Y_2^1 distribution, on the other hand, does dip in the forward direction. Under the assumption of the SS mechanism, this suggests that the p-wave background has a forward dip; in the KM view, the dip would be caused by the $M1$ helicity flip amplitude falling to zero in the forward direction.

E. The 1.35-GeV mass peak

The peak in nucleon–slow-pion mass at 1.35 GeV, shown in Fig. 7, has been observed in previous experiments,[1] but, because of its strong t dependence, has not been clearly resolved. A peak with similar t dependence has been observed recently in n-p collisions at 50–300 GeV/c.[17] No evidence is available on its persistence at ISR energies in pp collisions because of cuts in those data due to acceptance.[13]

From Fig. 9 we have observed from the Y_1^0 moment that the decay distribution in this region has a strong backward asymmetry in the t channel frame. We now explore the t dependence of the asymmetry. In Fig. 13 we show the Y_1^0, Y_1^1, and
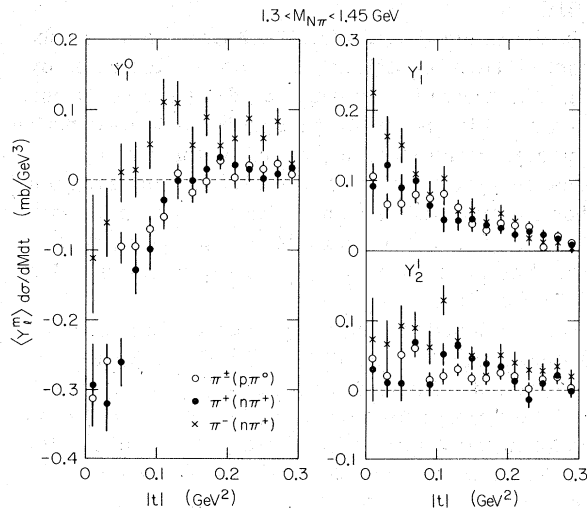
Y_2^1 moments against t for the region $1.3 < M_{N\pi} < 1.45$ GeV, (a) for the average of $+(p\pi^0)$ and $-(p\pi^0)$ (open circles), (b) for $+(n\pi^+)$ (closed circles), and (c) for $-(n\pi^+)$ (crosses). Here we note a marked similarity between $\pm(p\pi^0)$ and $+(n\pi^+)$ distributions, especially in the negative excursion in Y_1^0 at small t. The $-(n\pi^+)$ channel also shows a sharp drop in Y_1^0 at small t, superimposed on a larger background which presumably peaks at $t = 0$.

The interpretation of the 1.35-GeV mass peak as a resonance is highly improbable. We attempt to show this by the following reasoning:

1. The absence of a signal near 1.35 GeV in moments with $l \geqslant 2$ suggests that the resonance there can be only s or p wave. The Y_1^0 signal would then be interpreted as interference between s and p waves, one from the resonance, the other from the background, as in the case of the Δ interference patterns.

2. The backgrounds, as analyzed by Δ interference, show an $I = \frac{1}{2}$ characteristic, i.e., are twice as strong in the $(n\pi^+)$ as in the $(p\pi^0)$ channel. The supposed interference (Y_1^0 of Fig. 9) gives equal signals in $+(p\pi^0)$ and $-(p\pi^0)$ channels, so that both resonance and background would have to have $I = \frac{1}{2}$ if excited diffractively.

3. We therefore would expect twice the Y_1^0 signal to be found in the Y_1^0 moment in the $(n\pi^+)$ channels. In contrast to this, we note from Fig. 13 and Fig. 9 that the signals are approximately equal, assuming a smooth behavior of the background at small t.

The general forward asymmetry found in the data is well explained by the π-exchange DHD effect diagram of Fig. 1(b). The reversal of this trend at the 1.35-GeV mass peak is then most reasonably attributed to the baryon-exchange DHD effect diagram of Fig. 1(c), which is expected to produce a backward peaking,[1] once resonance excitation [Fig. 1(d)] is excluded. However, we have found no calculation of this contribution which produced the required sharpness of the peak, the slow rise from the nucleon-pion threshold, the t dependence, and the steepness of the backward peaking.

We will describe more of the characteristics of this mass region in Sec. VIII B.

F. Discussion of the interference patterns above 1.45 GeV

As noted in Sec. VI C part (e), there are strong indications in the moments for $M_{N\pi} > 1.45$ GeV that resonances are being excited diffractively. There are two mass values (at least) where the phase of particular waves are changing rapidly: i.e., $M_{N\pi} = 1.5$ GeV and $M_{N\pi} = 1.68$ GeV.

The best candidates for the two major resonances are the $D_{3/2}$ and $F_{5/2}N\pi$ resonances. These are allowed by the Morrison-Gribov (MG) rule[20] that in diffractive production, spin and parity should be

FIG. 13. Moments Y_1^0, Y_1^1, and Y_2^1 as functions of t in the mass interval $1.3 < M_{N\pi} < 1.45$ GeV, i.e., the 1.35-Gev peak. Open circles show the average of $\pi^\pm p \rightarrow \pi^\pm (p\pi^0)$, closed circles, $\pi^+ p \rightarrow \pi^+ (n\pi^+)$, and crosses, $\pi^- p \rightarrow \pi^- (n\pi^+)$.

related by $P = (-1)^{J-1/2}$. We wish to test the rule by looking for evidence of waves with the opposite relation.

The angular distributions, in terms of a partial-wave analysis, to be expected in our reactions have been calculated by Silver.[21] The reader is also referred to applications of explicit formulas in the literature.[22,23] For our purposes we have found it convenient to define production amplitudes $\mathcal{L}_T(M_{N\pi}, t)$ for the intermediate states which decay into an $N\pi$ system with angular momentum l. $\mathcal{L} = S, P, D, \ldots$, in the usual spectroscopy notation for l, and the subscript $T = M$ for the "MG allowed" states with $J = l - \frac{1}{2}$, $T = A$ for the "antirule" states with $J = l + \frac{1}{2}$. We also assume t-channel helicity conservation (TCHC). The result is

$$
\begin{aligned}
d\sigma/dM_{N\pi}dtd\Omega &= (4\pi)^{-1/2} \sum_{L=0}^{\infty} Y_L^0(\theta, \phi) \sum_{\text{all } \mathcal{L}_T, \mathcal{L}'_{T'}} B_L(\mathcal{L}_T, \mathcal{L}'_{T'}) \mathcal{L}_T^* \mathcal{L}'_{T'} \\
&= (4\pi)^{-1/2} \sum_{L=0}^{\infty} Y_L^0(\theta, \phi) \left[\sum_{\mathcal{L}_T} A_L(\mathcal{L}_T, \mathcal{L}_T) |\mathcal{L}_T|^2 + \sum_{\mathcal{L}'_{T'} > \mathcal{L}_T} A_L(\mathcal{L}_T, \mathcal{L}'_{T'}) 2\,\mathrm{Re}\,\mathcal{L}_T^* \mathcal{L}'_{T'} \right],
\end{aligned}
\tag{14}
$$

where the ordering is S_A, P_M, P_A, D_M, etc. The coefficients A_L are given in Table I.

In Eq. (14) we have explicitly separated interference signals $\propto 2\,\mathrm{Re}(\mathcal{L}_T^* \mathcal{L}'_{T'})$ from those $\propto |\mathcal{L}_T|^2$, because if one wave passes through resonance the $M_{N\pi}$ dependence of the former may show an easily discernible interference pattern, while the latter gives only a broad peaking. We also note that, if all terms in Eq. (14), proportional to one pair of interfering amplitudes, e.g., $2\,\mathrm{Re}\,(P_A^* D_M)$, are collected, the signals in different L's bear a fixed relationship given by Table I.

The fact that only Y_L^M's with $M = 0$ appear in Eq. (14) is a result of assuming exact TCHC. If the pair of waves producing the sharp interference pattern have TCHC-violating components, these will result in the appearance of parallel patterns in $M \neq 0$ moments, as was pointed out by Rushbrooke

TABLE I. Contributions to moment distributions for various interfering resonant states, assuming helicity conservation in production. For notation, see text.

Interfering states	Y_0^0	Y_1^0	Y_2^0	Y_3^0	Y_4^0	Y_5^0
$S_A S_A$ or $P_M P_M$	1					
$S_A P_M$		$-(\frac{1}{3})^{1/2}$				
$S_A P_A$ or $P_M D_M$		$(\frac{2}{3})^{1/2}$				
$P_A P_A$ or $D_M D_M$	1		$(\frac{1}{5})^{1/2}$			
$S_A D_M$ or $P_A P_M$			$-(\frac{2}{5})^{1/2}$			
$S_A D_A$ or $P_M F_M$			$(\frac{3}{5})^{1/2}$			
$S_A F_A$ or $P_M G_M$		0		$(\frac{4}{7})^{1/2}$		
$S_A F_M$ or $P_M D_A$		0		$-(\frac{3}{7})^{1/2}$		
$P_A D_A$ or $D_M F_M$		$\frac{3}{5}\sqrt{2}$		$\frac{2}{5}(\frac{6}{7})^{1/2}$		
$P_A D_M$		$-\frac{1}{5}(\frac{1}{3})^{1/2}$		$-\frac{9}{5}(\frac{1}{7})^{1/2}$		
$D_A D_A$ or $F_M F_M$	1		$\frac{3}{7}(\frac{1}{5})^{1/2}$		$\frac{2}{7}$	
$P_A F_M$ or $D_A D_M$			$-\frac{1}{7}(\frac{6}{5})^{1/2}$		$-\frac{2}{7}\sqrt{6}$	
$P_M F_A$ or $S_A G_M$			0		$-\frac{2}{3}$	
$P_A F_A$ or $D_M G_M$			$\frac{9}{7}(\frac{2}{5})^{1/2}$		$\frac{5}{21}\sqrt{2}$	
$D_A F_M$		$-\frac{1}{35}\sqrt{3}$		$3(\frac{1}{7})^{1/2}$		$-\frac{50}{21}(\frac{1}{11})^{1/2}$
$D_M F_A$ or $P_A G_M$		0		$\frac{11}{3}(\frac{2}{7})^{1/2}$		$-\frac{5}{3}(\frac{2}{11})^{1/2}$
$D_A F_A$ or $F_M G_M$		$\frac{6}{7}$		$\frac{2}{3}(\frac{3}{7})^{1/2}$		$\frac{10}{21}(\frac{3}{11})^{1/2}$

et al.[23] Judging by the relatively small $M \neq 0$ signals apparent in our data (see Fig. 9), we expect Eq. (14) to be a good approximation if we look for resonance signals above background.

If we wish to assign F_M to the 1.68-GeV resonance, we find the absence of a positive Y_4^0 peak of $4/\sqrt{5}$ the Y_2^0 value disconcerting. The Y_3^0 signal might arise from an $D_M F_M$ interference, but this requires a parallel Y_1^0 signal of opposite sign to that observed. We also note that the presence of a Y_6^0 interference signal indicates that even higher waves than shown in the table may contribute strongly. Finally, Y_3^0 shows an anomalous behavior in the $-(p\pi^0)$ channel at 1.68 GeV, suggesting that $I = 1$ exchange also contributes here.

We may see from Table I that the assignment of D_M (i.e., $\frac{3}{2}^-$ state) at 1.5 GeV gives the Y_2^0 peak, and allows the presence of P_M to explain the Y_1^0 interference signal. The Y_4^0 interference signal requires D_A or G_M (the latter, however, requires an even larger Y_2^0 interference term). The same result comes if P_A is substituted for D_M, S_A for P_M, and F_M for D_A. In all such configurations some MG violating amplitudes are required.

VII. REACTIONS $\pi^\pm p \to \pi^\pm p\pi^+\pi^-$

We now consider the reactions

$$\pi^\pm p \to \pi^\pm (p\pi^+\pi^-). \tag{15}$$

In Figs. 14(a) and 14(b) we show the mass $M_{p\pi^+\pi^-}$, recoiling against the fast forward $\pi^\pm$ triggering particle by open and closed circles. The distributions are dominated by a broad peak at about 1.7 GeV which has been reported by many previous authors in these and other reactions.[24] In particular, the $p\pi^+\pi^-$ spectrum has been observed in pp collisions at ISR energies[25] to have substantially the same shape as shown here.

In Figs. 14(c) and 14(d) the $p\pi^+$ mass distribution is shown by open and closed circles. These indicate a strong $\Delta^{++}(1232)$ component is present. The crosses show the $M_{p\pi^-}$ distributions, indicating that the Δ peak is not a kinematic effect. We define the Δ by a cut, $M_{p\pi^+} < 1.34$ GeV, and estimate that about 25% non-Δ background will be included by the cut. Finally, the $M_{\Delta\pi}$ distribution is shown in Figs. 14(a) and 14(b) by crosses.

VIII. COMPARISON OF p, n, AND Δ FINAL STATES

A. Mass-slope correlation

We now investigate the mass-slope correlation of the diffractive enhancement for the $\pm(N\pi)$ and $\pm(\Delta\pi)$ channels. For this study we have fitted the $d\sigma/dMdt$ distribution for mass intervals of 20 MeV to an exponential form e^{Bt}, selecting the broadest t
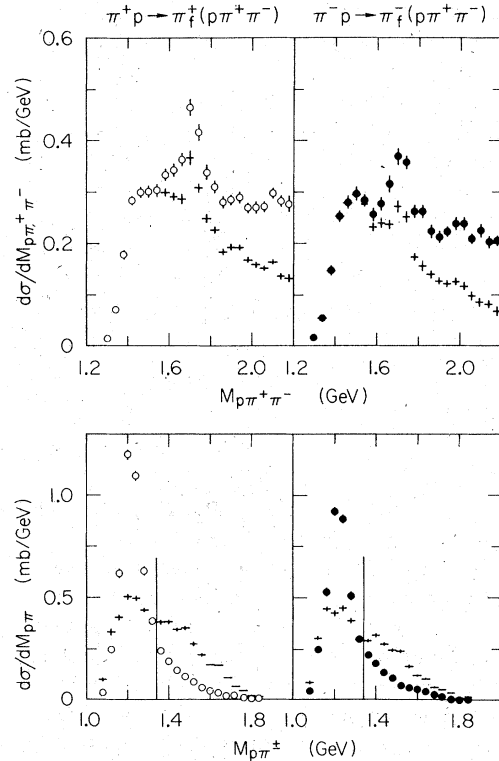

FIG. 14. (a) Invariant mass $M_{p\pi^+\pi^-}$ for the reaction $\pi^+ p \to \pi_f^+(p\pi^+\pi^-)$ before the Δ-defining cut (circles) and after the cut (crosses), (b) same for π^- beam, (c) $M_{p\pi^+}$ for the data of part (a) with $M_{p\pi^+\pi^-} < 2$ GeV (circles), showing the strong Δ^{++} signal. Vertical line shows the cut position used. Crosses show $M_{p\pi^-}$, which shows the peak is not kinematic in origin, (d) same for π^- beam.

range which can be described by this form. In Fig. 15 we show the results for the $(N\pi)$ and $(\Delta\pi)$ channels separately.

From this data we make two observations. First, the systematic increase in slope as mass decreases breaks off at about 1.35 GeV in the $(N\pi)$ channels, remains constant, and resumes rising below the $\Delta(1232)$ mass. While much of this is related to the presence of the nondiffractively produced Δ, the width of the plateau is too great and the amount of Δ production is too small to explain it entirely.

Secondly, we observe that, at a given mass, the slope in the $(\Delta\pi)$ channels is systematically higher than the slope in the $(N\pi)$ channels by about 4 units (GeV^{-2}) in the π^+-induced reactions and about 2.5 units in the π^--induced reactions. This indicates that at least part of the observed diffraction bump must be produced by a mechanism in which the "decay" is not independent of "production." We note that previous authors[26] investigating inelastic meson diffraction have found that "the slope of the $d\sigma/dt$ distribution is determined by the invariant
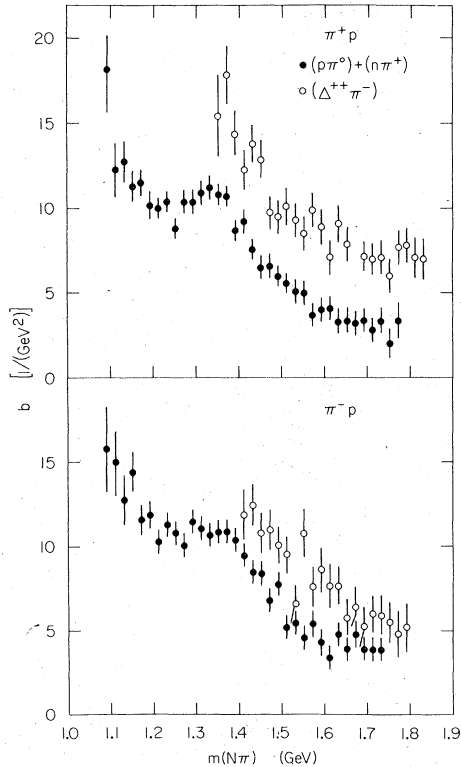
FIG. 15. "Mass-slope correlation," showing the slope parameter b, assuming $d\sigma/dMdt \propto e^{Bt}$ as a function of recoil mass, for the average of $(p\pi^\circ)$ and $(n\pi^+)$ channels, and the $(\Delta\pi)$ channel, (a) for the π^+ experiment, (b) for π^-.

mass produced, irrespective of the kind of particles carrying such masses."

B. Representation of decay distributions by isocline plots

The previous discussions of the properties of diffractively produced systems has suggested that, although resonances are present, they do not explain the dominant features of the data. In that case the moment distributions presented may not give the most useful description of the data.

Furthermore, there has recently been renewed interest in double-peripheral calculations, stimulated by the (relative) success of Ascoli *et al.*[27] in explaining the reaction $\pi p \rightarrow (3\pi)p$ by the Reggeized Drell-Hiida-Deck model, and by experimental data on nucleon diffraction.[17,26] Miettinen[1] has suggested the use of "isocline plots," where the (θ, ϕ) distributions are replaced by contours of equal-event densities, to locate contributions from these processes.

The technique we have used to produce such plots is to evaluate the moments defined by Eq. (12) up to $l = 4$ and $m = 2$ and use the resulting mathematical representation to find the isoclines[28] in the in-

terval $0.01 < |t| < 0.5$ GeV^2. Here we shall show only the π^+-beam results, since the π^- data are qualitatively the same, and because no significant azimuthal asymmetry was observed, we have folded the data about $\phi = 0$. Owing to the use of $l \le 4$, the results are smoothed in a manner appropriate to the analysis of Miettinen.[1]

Figure 16 shows the plots for the two lower mass intervals, $1.08 < M_{N\pi} < 1.3$ GeV and $1.3 < M_{N\pi} < 1.45$ GeV. The isoclines are labeled by the event density $8\pi d\sigma/dMd\Omega$ in mb GeV^{-1}.

The peaking seen near $\cos\theta = 1$, $\phi = 0$ can be attributed to the π-exchange DHD process of Fig. 1(b). Since $\cos\theta$ is linearly related to the 4-momentum transfer squared from target to nucleon Δ^2, the $\cos\theta$ distribution directly reflects the Δ^2 distribution in π exchange. $\phi = 0$ corresponds to the largest $M_{\pi\pi}$ which can be achieved at fixed θ. High $M_{\pi\pi}$ values are enhanced by the π exchange process and are concentrated into the low-$M_{N\pi}$ region, resulting in low ϕ values being favored.[1]

The backward peaking in θ can be seen best in Figs. 16(c) and 16(d). It shows a comparatively weak ϕ dependence. These distributions compare well with the patterns expected for baryon exchange, when nuclear spin is taken into account.[5,6] This is strong, though not conclusive, evidence
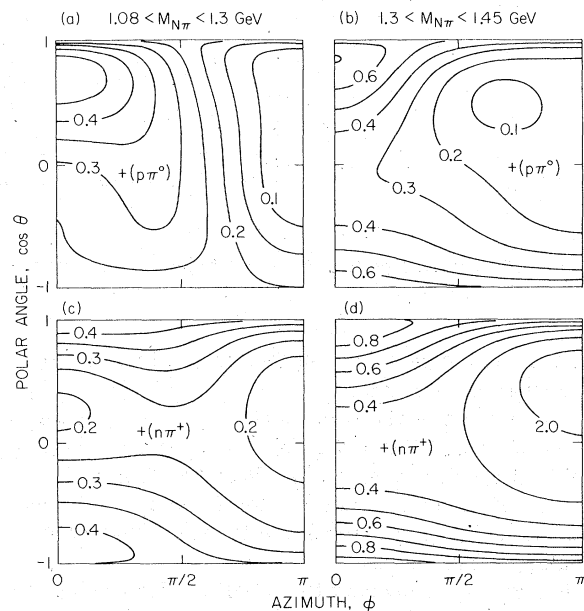

FIG. 16. Isocline plots, i.e., contours of equal event densities against $\cos\theta$ and ϕ in the t-channel frame, for the two lower recoil-mass intervals and reaction channels shown, obtained as described in the text. Contours are labeled by the density in the text. Contours are labeled by the density in mb/GeV, as obtained in the interval $0.01 < |t| < 0.5$ GeV^2.
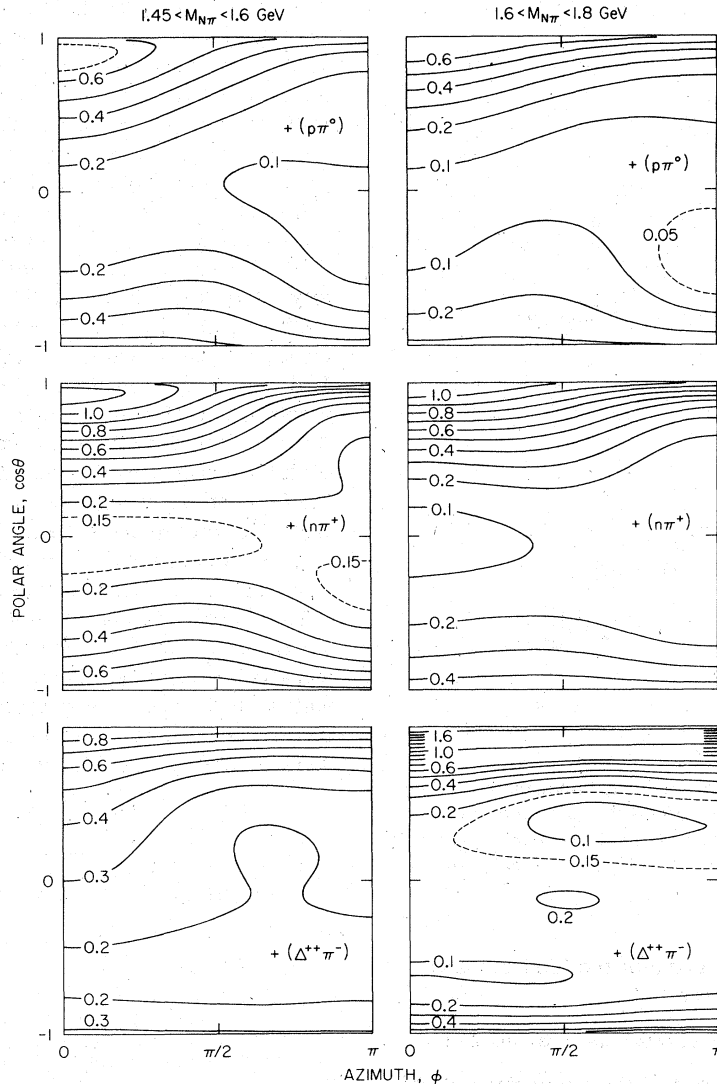
FIG. 17. Isocline plots for the two higher-mass intervals shown and including the $(\Delta\pi)$ channels, labeled as in Fig. 16.

that the mass peak at 1.35 GeV is due to a baryon-exchange mechanism.

The effects of the Δ production process can be seen in Figs. 16(a) and 16(b), where the Stodolsky-Sakurai distribution, $1 + 3 \sin^2\theta \sin^2\phi$, fills in the center of the plot, and the interference term mentioned previously changes the forward-backward peaking considerably.

In Fig. 17 we present the isoclines for the higher mass intervals shown, and include the $+(\Delta^{++}\pi^-)$ channels for comparison. Compared to the previous figure, we see that the π exchange peaking is much sharper now, as the range of Δ^2 in the plot is greater, but the integrated effect is much less. The backward peak continues to fall with increasing mass in the $N\pi$ channels. However, we note

that no very strong backward peak appears in the $\Delta\pi$ channel until we reach the interval containing the 1700-MeV peak.

C. Correlation of mass with decay angle

A complementary method to study the double-peripheral mechanism and presence of more than one exchange is to study the correlation of the production slope with the decay angular distribution (Ref. 29). The authors of Ref. 30 claim an observation of a crossover effect in $d\sigma/dt$ with the sign depending on whether the pion or the baryon exchange was enhanced.

In order to study these questions in detail, we present in Fig. 18 the "reaction mass-slope decay correlations": The mass spectra and the mass de-
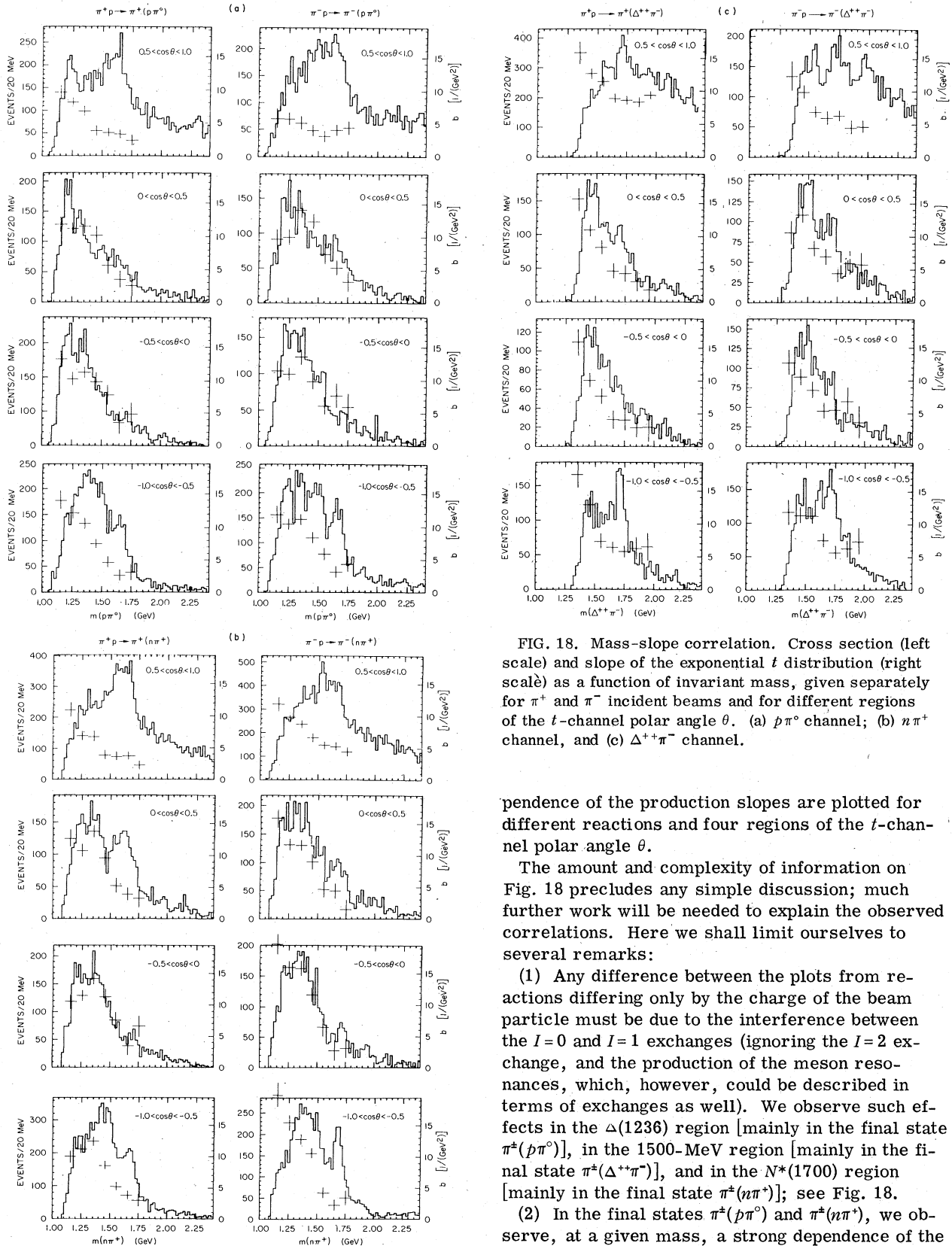
FIG. 18. Mass-slope correlation. Cross section (left scale) and slope of the exponential t distribution (right scale) as a function of invariant mass, given separately for π^+ and π^- incident beams and for different regions of the t-channel polar angle θ. (a) $p\pi^\circ$ channel; (b) $n\pi^+$ channel, and (c) $\Delta^{++}\pi^-$ channel.

pendence of the production slopes are plotted for different reactions and four regions of the t-channel polar angle θ.

The amount and complexity of information on Fig. 18 precludes any simple discussion; much further work will be needed to explain the observed correlations. Here we shall limit ourselves to several remarks:

(1) Any difference between the plots from reactions differing only by the charge of the beam particle must be due to the interference between the $I=0$ and $I=1$ exchanges (ignoring the $I=2$ exchange, and the production of the meson resonances, which, however, could be described in terms of exchanges as well). We observe such effects in the $\Delta(1236)$ region [mainly in the final state $\pi^\pm(p\pi^\circ)$], in the 1500-MeV region [mainly in the final state $\pi^\pm(\Delta^{++}\pi^-)$], and in the $N^*(1700)$ region [mainly in the final state $\pi^\pm(n\pi^+)$]; see Fig. 18.

(2) In the final states $\pi^\pm(p\pi^\circ)$ and $\pi^\pm(n\pi^+)$, we observe, at a given mass, a strong dependence of the

production slopes on $\cos\theta$, especially in the mass region of 1.2–1.5 GeV. A similar, even stronger effect has been observed in the reaction $pp \to p(n\pi^+)$ at the ISR (Ref. 13) and also in diffractive dissociation of high-energy neutrons on protons at Fermilab (Ref. 17). This behavior is qualitatively predicted by the double-peripheral model.

(3) In general, the slope-mass correlation is much stronger in the backward than in the forward region of $\cos\theta$; the two extreme cases being the decrease of the slope by $\simeq 18$ units over a mass range of $\simeq 500$ MeV in the backward region of the reaction $\pi^- p \to \pi^-(n\pi^+)$ and the nearly mass-independent slope in the forward region of the reaction $\pi^- p \to \pi^-(p\pi^\circ)$. It is also interesting to note that the slope for the reaction $\pi^+ p \to \pi^+(\Delta^{++}\pi^-)$ levels off at a relatively large value of ~9.0 at large $m(\Delta\pi)$.

(4) We do not observe a simple change of the sign of the crossover in the reactions $\pi^\pm p \to \pi^\pm$ $(\Delta^{++}\pi^-)$, when the pion-exchange ($\cos\theta > 0$) or the baryon exchange ($\cos\theta < 0$) is enhanced. Attempts to enhance the different exchanges by selecting regions of the azimuthal s-channel angle (the method used by the authors of Ref. 30) also failed to reproduce the reported effect.

(5) Besides the $\Delta^+(1236)$, the other substructures observed in the data are in the 1600–1700-MeV region, and there is a poorly defined structure around 1500 MeV. The 1700-MeV region is especially interesting: It seems to contain contributions from several states, including a narrow peak at ~1700 MeV [see, e.g., the backward part of the reaction $\pi^+ p \to \pi^+(\Delta^{++}\pi^-)$ on Fig. 18]. There are six established baryon resonances in the 1650–1700-MeV

region, but the width of the narrowest of them is greater than observed here.

Evidence for a narrow object at 1700 MeV was already observed at 3.9 GeV/c in the backward-produced $(p\pi)$ system in the reaction $\pi^- p \to (p\pi^-)\omega$ and in the reaction $\pi^- p \to \pi^-(p\pi^+\pi^-\pi^\circ)$.[31]

IX. CONCLUSIONS

We have presented the data from our high-statistics hybrid-bubble-chamber experiments at 14 GeV/c. These data reveal a very complex behavior which cannot be explained by one dominant mechanism. We have, therefore, presented the data itself and limited our discussions to its qualitative aspects.

We have observed a broad mass peak in the $\pm(N\pi)$ channels at 1.35 GeV. Its isospin and decay characteristics make it unlikely to be due to resonance production.

Sharp changes with $M_{N\pi}$ observed in the moments of the decay angular distribution at higher masses indicate the production of resonances. However, these cannot be explained by introduction of amplitudes obeying only the Gribov-Morrison rule.[20]

We find that the mass-slope correlation in our data depends on the particular final state, in contrast to the results obtained in diffractive boson production.

ACKNOWLEDGMENTS

*On leave from C. E. N. de Saclay.
†Present address: Mons University, Mons, Belgium.
‡Present address: CERN, Geneva, Switzerland.
§Present address: Iowa State University, Ames, Iowa.
[1]For recent reviews of the subject see: H. Miettinen, in *High Energy Physics*, proceedings of the European Physical Society International Conference, Palermo, 1975, edited by A. Zichichi (Editrice Compositori, 1976); M. Derrick, in *Particles and Fields—1975*, proceedings of the meeting of the Division of Particles and Fields of the APS, Seattle, edited by H. J. Lubatti and P. M. Mockett (Univ. of Washington, Seattle, 1976), p. 33.
[2]S. D. Drell and K. Hiida, Phys. Rev. Lett. 7, 199 (1961).
[3]R. Deck, Phys. Rev. Lett. 13, 1969 (1964).
[4]V. A. Tsarev, Phys. Rev. D 11, 1864 (1975).
[5]A. Minaka et al., Prog. Theor. Phys. 57, 169 (1977).
[6]R. Cutler and E. Berger, Phys. Rev. D 15, 1903 (1977).
[7]A. R. Dzierba et al., Phys. Rev. D 7, 725 (1973); L. Rosenfeld, Ph.D. thesis, California Institute of Technology, 1977 (unpublished).
[8]K. J. Foley et al., Phys. Rev. 181, 1775 (1969).
[9]J. V. Beaupré et al., Nucl. Phys. B66, 93 (1973).

[10]J. H. Scharenguivel et al., Nucl. Phys. B36, 363 (1972).
[11]The Δ^+ cross section used here may be too low, based upon interpolation of other data to our energy, and upon an independent fit to our $\pm(p\pi^\circ)$ channels. Using a higher cross section would result in a more enhanced 1.35-GeV peak and a steeper t slope for events under the Δ.
[12]E. Nagy et al., contribution No. 489 to the XVIIth International Conference on High Energy Physics, London, 1974 (unpublished).
[13]H. de Kerret et al., Phys. Lett. 63B, 477 (1976); 63B, 483 (1976); C. Broll, Orsay Report No. 1580 (doctoral thesis, 1976) (unpublished).
[14]G. B. Chadwick, *Particles and Fields—1975* (see Ref. 1), p. 197.
[15]J. D. Jackson, Rev. Mod. Phys. 37, 484 (1965).
[16]W. Ochs et al., Nucl. Phys. B86, 253 (1975).
[17]J. Biel et al., Phys. Lett. 65B, 291 (1976); Phys. Rev. Lett. 36, 504 (1976); 36, 507 (1976).
[18]L. Stodolsky and J. Sakurai, Phys. Rev. Lett. 11, 90 (1963).
[19]M. Krammer and U. Maor, Nucl. Phys. B13, 651

(1969).

[20]V. N. Gribov, Yad. Fiz. 5, 197 (1967); D. R. O. Morrison, Phys. Rev. 165, 1699 (1968).

[21]R. N. Silver, thesis, California Institute of Technology, 1971 (unpublished).

[22]D. Lissauer *et al.*, Phys. Rev. D 6, 1852 (1972).

[23]J. G. Rushbrooke *et al.*, Phys. Rev. D 13, 1835 (1976).

[24]Many results are tabulated by K. Boesebeck *et al.*, Nucl. Phys. B33, 445 (1971). More recent observations above 10 GeV/c are (a) π-nucleon: R. Morse *et al.*, Phys. Rev. D 4, 133 (1971); Y. Oh *et al.*, Phys. Lett. 42B, 497 (1972); R. Harris *et al.*, University of Washington Report No. VTL PUB-22, 1975 (unpublished); (b) nucleon-nucleon: J. Allaby *et al.*, Nucl. Phys. B52, 316 (1973); D. Hochman *et al.*, *ibid.* B80, 45 (1974).

[25]R. Webb *et al.*, Phys. Lett. 55B, 331 (1975).

[26]P. Bosetti *et al.*, Nucl. Phys. B101, 304 (1975).

[27]G. Ascoli *et al.*, Phys. Rev. D 8, 3894 (1973); 9, 1963 (1974).

[28]The subroutine used, CONTRG, was written by R. Beebe of the SLAC computation group.

[29]E. L. Berger, Phys. Rev. D 11, 3214 (1975), and *Proceedings of Daresbury Study Weekend No. 8, 1975,* edited by J. B. Dainton and A. J. G. Hey (Science Research Council, Daresbury, England, 1975); H. Miettinen, Ref. 1; D. W. Duke, Lett. Nuovo Cimento 19, 660 (1977).

[30]P. Bosetti *et al.*, Nucl. Phys. B103, 189 (1976).

[31]V. Davidson *et al.*, Phys. Rev. Lett. 32, 855 (1974); V. Chaloupka, Ph.D. thesis, University of Geneva, 1975 (unpublished).